Preprints of the 21st IFAC World Congress (Virtual)
Berlin, Germany, July 12-17, 2020

Performance Comparison between Triple-stage Actuator Systems in HDDs

Takenori Atsumi * **Shota Yabui** **

* *Chiba Institute of Technology, Narashino, Chiba, 275-0016 Japan (e-mail: takenori.atsumi@p.chibakoudai.jp)*
** *Nagoya University, Nagoya, Aichi, 464-8603 Japan (e-mail: yabui@nuem.nagoya-u.ac.jp)*

Abstract: In this paper, we present a comparison study between three triple-stage actuator systems of the magnetic-head positioning system in hard disk drives (HDDs). As of year 2019, we have four kinds of actuators for the magnetic-head positioning system: voice coil motor ("VCM"), "Milli" actuator with two piezoelectric (PZT) elements, "Micro" actuator with two PZT elements, and a "Thermal" actuator that consists of heaters embedded in the magnetic head and move read/write elements a few nanometers in a horizontal direction with thermal expansion. This means that we are able to build three kinds of triple-stage actuator systems: "VCM + Milli + Micro", "VCM + Milli + Thermal", and "VCM + Micro + Thermal". In order to find the best triple-stage actuator system for upcoming 1000 kTPI (track pitch: 25 nanometer) HDD era, we examine case studies and estimate the position error signals and movements of actuators of the track-following control systems under the external vibration in a file server. In this case study, it is shown that achievable disturbance-rejection performances of these triple-stage-actuator systems depend on not only the frequency responses the actuators but also the stroke limitations of the actuators. As a result, we found that the triple-stage actuator system that consist of the VCM, the Milli actuator, and the Micro actuator has the best performance for 1000 kTPI HDD.

Keywords: Precision control, Data storage, Positioning systems, Actuators, Servo.

1. INTRODUCTION

To increase data capacity of hard disk drives (HDDs), we have to improve positioning accuracy of magnetic heads in the HDDs so that size of bits for information stored on a disk decreases (Abrahamson and Fu-ying (2015)). Thus, in the magnetic-head positioning system, we have to increase a servo bandwidth of the control system. However, the mechanical characteristics limit the servo bandwidth (Yamaguchi and Atsumi (2008)). Therefore, the magnetic-head positioning system should be fabricated with multiple actuators so that the servo bandwidth can be increased (Atsumi (2016)).

For the magnetic-head positioning system, we have reported that a triple-stage actuator system was dramatically able to improve the positioning accuracy during a track-following control from the dual-stage actuator systems (Atsumi et al. (2013)). As of year 2019, we have four kinds of actuators for the magnetic-head positioning system: voice coil motor ("VCM"), "Milli" actuator with two piezoelectric (PZT) elements, "Micro" actuator with two PZT elements, and "Thermal" actuator that consists of heaters embedded in the magnetic head and move read/write elements a few nanometers in a horizontal direction with thermal expansion. This means that we are able to build three kinds of triple-stage actuator systems: "VCM + Milli + Micro", "VCM + Milli + Thermal", and "VCM + Micro + Thermal".

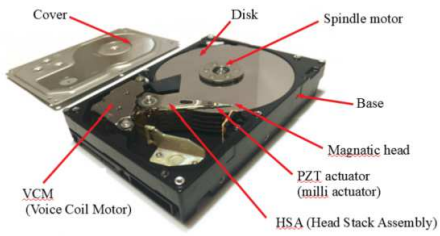

Fig. 1. Picture of current shipped HDD.

In this paper, we present a comparison study between the three triple-stage actuator systems in HDDs. In order to find the best triple-stage actuator system for 1000 kTPI (track pitch: 25 nanometer) HDD era, we examine case studies and estimate the position error signals and movements of actuators of the track-following control systems under the external vibration in a file server.

2. MAGNETIC-HEAD POSITIONING SYSTEM

A current shipped HDD is comprised of a cover, a base, a VCM, several PZT actuators, several magnetic heads, several disks, a spindle motor, and a head-stack assembly (HSA), as shown in Fig. 1. Magnetic heads are on the suspensions in the HSA. The HSA has a coil of the VCM, PZT elements, and the magnetic heads. The magnetic-head position signal is generated from embedded information in servo sectors located at regular intervals on the disks. Therefore, the magnetic-head position signal is

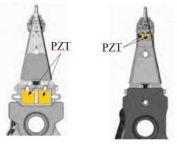

(a) (b)

Fig. 2. Structures of PZT actuators: (a) Milli actuator and (b) Micro actuator.

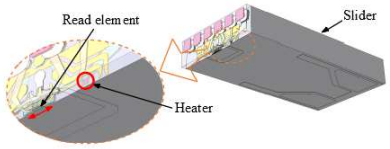

Fig. 3. Basic schematic diagram of Thermal actuator.

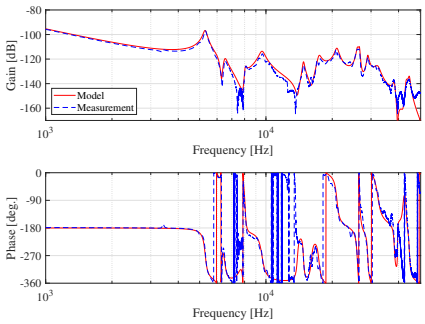

Fig. 4. Frequency response of P_{vcm}.

only available as a discrete-time signal at a sampling time determined by the number of servo sectors and the rotation rate of the spindle motor (Atsumi and Messner (2013)).

Fig. 2 (a) shows a structure of the Milli actuator, and Fig. 2 (b) shows a structure of the Micro actuator. The Milli actuator is the first generation of a secondary actuator for a dual-stage actuator in the shipped HDDs, and uses a sway motion in the suspension. The Micro actuator is the second generation of the secondary actuator for the dual-stage actuator in the shipped HDDs, and uses a yaw motion in the suspension. Therefore, the frequency of the primary mechanical resonance of the Micro actuator is much higher than that of the Milli actuator (HGST (2017)). On the other hand, a stroke limitation of the Micro actuator is shorter than that of the Milli actuator.

Fig. 3 shows a basic schematic diagram of the Thermal actuator in the magnetic head. In this system, a heater is located in a horizontal direction of the read/write elements. The control system can move the position of read/write elements a few nanometers in a horizontal direction with thermal expansion caused by heaters. The magnetic-head positioning system with the Thermal actuator enables us to control the magnetic-head position in high-frequency range because the Thermal actuator system has no mechanical resonant mode. On the other hand, its stroke limitation is too short to compensate for disturbances at low frequency.

In this study, we employed characteristics of the VCM and the Milli actuator shown in reference, Atsumi et al. (2015).

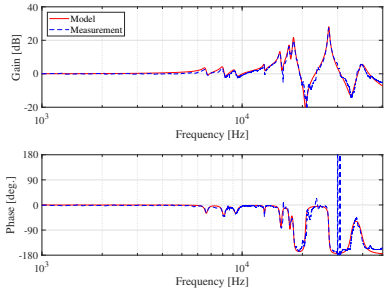

Fig. 5. Frequency response of P_{mil}.

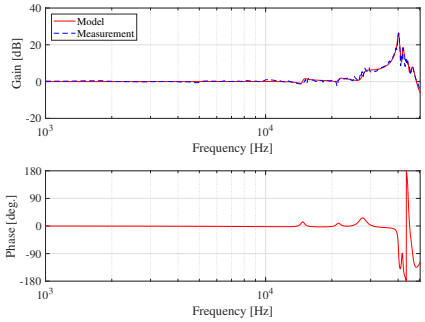

Fig. 6. Frequency response of P_{mic}.

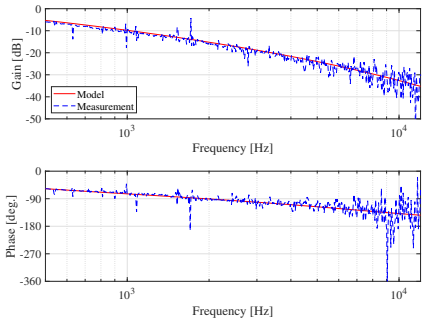

Fig. 7. Frequency response of P_{the}.

The measured frequency response of the VCM is shown as dashed lines in Fig. 4. The frequency response of the mathematical model of the VCM, $P_{vcm}(s)$, is shown as solid lines in Fig. 4. The measured frequency response of the Milli actuator is shown as dashed lines in Fig. 5. The frequency response of the mathematical model of the Milli actuator, $P_{mil}(s)$, is shown as solid lines in Fig. 5.

In this study, we employed characteristics of the Micro actuator shown in reference, HGST (2017). The measured frequency response of the Micro actuator is shown as dashed lines in Fig. 6. The frequency response of the mathematical model of the Micro actuator, $P_{mic}(s)$, is shown as solid lines in Fig. 6.

In this study, we employed characteristics of the Thermal actuator shown in reference, Atsumi et al. (2013). The dashed lines in Fig. 7 show a frequency response of the Thermal actuator. The frequency response of the mathematical model of the Thermal actuator, $P_{the}(s)$, is shown as solid lines in Fig. 7.

In the magnetic-head positioning control system, the PZT and Thermal actuators have stroke limitations (effective displacement). The stroke limitations depend on the actu-

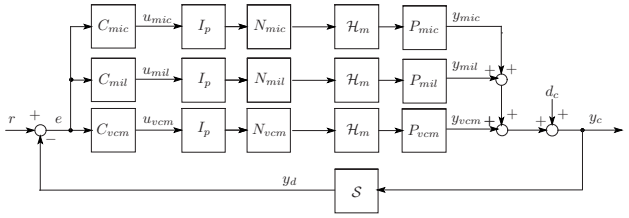

Fig. 8. Block diagram of control system in Case 1.

ator design. And the actuator design depends on a target track pitch of the control system. In this study, we assumed that the target track pitch is less than 25.3 nm (more than 1000 kTPI). Therefore, we also assumed that the stroke limitations are as follows.

- Milli actuator: 100 nm.
- Micro actuator: 20.0 nm.
- Thermal actuator: 1.00 nm.

3. CONTROL SYSTEM DESIGN

In this section, we design control systems for three kinds of triple-stage actuator systems: "VCM + Milli + Micro", "VCM + Milli + Thermal", and "VCM + Micro + Thermal". In this study, we assume that these actuators have no coupling with other actuators.

3.1 Case 1: "VCM + Milli + Micro"

Fig. 8 shows a block diagram of a magnetic-head positioning control system with the triple-stage-actuator that consists of the VCM, the Milli actuator, and the Micro actuator. Here, C_{vcm} is a feedback controller for the VCM, N_{vcm} is a multi-rate notch filter for the VCM, C_{mil} is a feedback controller for the Milli actuator, N_{mil} is a multi-rate notch filter for the Milli actuator, C_{mic} is a feedback controller for the Micro actuator, N_{mic} is a multi-rate notch filter for the Micro actuator, $\mathcal{S}$ is a sampler, $\mathcal{H}$ is a zero-order hold (ZOH), $\mathcal{H}_m$ is a multi-rate ZOH, and I_p is an interpolator. d_c is a disturbance signal for the magnetic-head positioning system, r indicates a reference signal for the magnetic-head positioning system, e indicates an error signal for the magnetic-head positioning system, y_c indicates the magnetic-head position in continuous time, and y_d indicates the measured magnetic-head-position signal in discrete time. u_{vcm} is an output signal from C_{vcm}, u_{mil} is an output signal from C_{mil}, u_{mic} is an output signal from C_{mic}, y_{vcm} is an output signal from P_{vcm}, y_{mil} is an output signal from P_{mil}, and y_{mic} is an output signal from P_{mic}.

In the $\mathcal{S}$ and $\mathcal{H}$, a sampling time T_s is 19.84 μs (the sampling frequency ω_s is 50.40 kHz). In the I_p, N_{vcm}, N_{mil}, N_{mic}, and $\mathcal{H}_m$, the sampling time is 9.92 μs (a multi-rate number is two). In this study, the interpolator $I_p[z]$ consists of an up-sampler and an interpolation filter. Thus, $I_p[z]$ can be given as follows.

$$I_p[z] = \sum_{m=1}^{2} z^{1-m}. \tag{1}$$

The transfer characteristics from u_{vcm} to y_d at ω_0, which is the open-loop characteristics for the VCM in a discrete-time system, is given as follows (Atsumi (2010)).

$$L_{vcm}[\omega_0] = C_{vcm}[e^{j\omega_0 T_s}]P_{dvcm}[\omega_0], \tag{2}$$

where

$$\begin{aligned} P_{dvcm}[\omega] &= \frac{1}{T_s}\sum_{k=-\infty}^{\infty} W_{vcm}[\omega+\omega_s k]P_{vcm}(j\omega+j\omega_s k), \\ W_{vcm}[\omega] &= I_p[e^{j\omega\frac{T_s}{2}}]N_{vcm}[e^{j\omega\frac{T_s}{2}}]\mathcal{H}_m(j\omega). \end{aligned} \tag{3}$$

Note that the L_{vcm} includes the continuous-time plant, the multi-rate ZOH, the multi-rate notch filter, the feedback controller for the VCM, and the sampler. Similarly, open-loop characteristics for the Milli actuator (L_{mil}) and open-loop characteristics for the Micro actuator (L_{mic}) can be given as follows.

$$\begin{aligned} L_{mil}[\omega_0] &= C_{mil}[e^{j\omega_0 T_s}]P_{dmil}[\omega_0], \\ L_{mic}[\omega_0] &= C_{mic}[e^{j\omega_0 T_s}]P_{dmic}[\omega_0], \end{aligned} \tag{4}$$

where

$$\begin{aligned} P_{dmil}[\omega] &= \frac{1}{T_s}\sum_{k=-\infty}^{\infty} W_{mil}[\omega+\omega_s k]P_{mil}(j\omega+j\omega_s k), \\ P_{dmic}[\omega] &= \frac{1}{T_s}\sum_{k=-\infty}^{\infty} W_{mic}[\omega+\omega_s k]P_{mic}(j\omega+j\omega_s k), \\ W_{mil}[\omega] &= I_p[e^{j\omega\frac{T_s}{2}}]N_{mil}[e^{j\omega\frac{T_s}{2}}]\mathcal{H}_m(j\omega), \\ W_{mic}[\omega] &= I_p[e^{j\omega\frac{T_s}{2}}]N_{mic}[e^{j\omega\frac{T_s}{2}}]\mathcal{H}_m(j\omega). \end{aligned} \tag{5}$$

An open-loop characteristics in the triple-stage actuator system (L_{tsa}) and a sensitivity function (S_{tsa}) are given as follows:

$$L_{tsa} = L_{vcm} + L_{mil} + L_{mic}, S_{tsa} = \frac{1}{1+L_{tsa}}. \tag{6}$$

In the magnetic-head positioning control system, saturations of actuators worsen the performance of the control system (Herrmann et al. (2004)). In this study, we focused on the track-following control under the external vibration. In this case, we must prevent actuator saturations because the disturbance-rejection performance must be kept during the track-following control. In order to consider the stroke limitations of actuators, we should set an upper limit of the H-infinity norm of the transfer characteristics from the disturbance signal (d_c) to an output signal from the PZT actuators (y_{mil} and y_{mic}). It is called "Stroke function" hereafter. The stroke functions for the Milli actuator (R_{mil}) and that for the Micro actuator (R_{mic}) can be given by following equations.

$$R_{mil} = L_{mil}\cdot S_{tsa}, R_{mic} = L_{mic}\cdot S_{tsa}. \tag{7}$$

To make the control system stable with an enough margin, we have set the upper limit of $||S_{tsa}||_\infty$ as 6 dB. In order not to exceed the stroke limitations of the actuators, we have also set the upper limit of $||R_{mil}||_\infty$ as 12 dB, and that of the $||R_{mic}||_\infty$ as 6 dB.

The multi-rate notch filters (N_{vcm}, N_{mil}, and N_{mic}) have to decrease the gains at the mechanical resonances beyond the Nyquist frequency of the sampler $\mathcal{S}$. As a result, these multi-rate notch filters are given as shown in Fig. 9 (dashed: N_{vcm}, dot-dashed: N_{mil}, solid: N_{mic}).

C_{vcm} has to stabilize a rigid-body mode of the VCM by a phase-lead element, and provide an integral action. It also has to stabilize mechanical resonances at 5.3 kHz and 9.6 kHz (the butterfly modes) by a phase-delay element. As a result, C_{vcm} is given as shown as solid lines in Fig. 10.

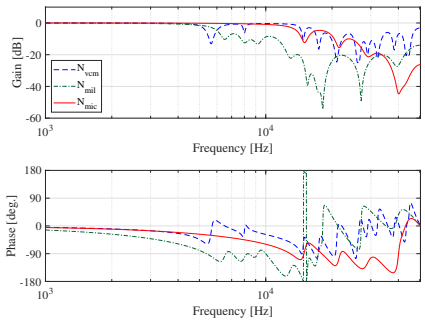

Fig. 9. Frequency responses of N_{vcm}, N_{mil}, and N_{mic}.

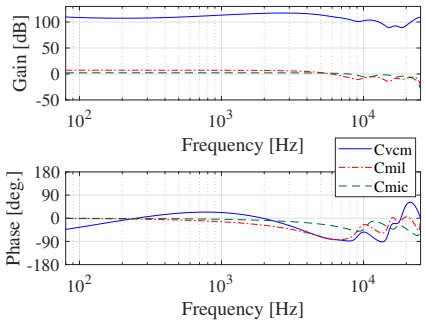

Fig. 10. Frequency responses of C_{vcm}, C_{mil}, and C_{mic} in Case 1.

Note that the L_{vcm} (open-loop for VCM) has unstable characteristics from 2 to 4 kHz.

C_{mil} has to compensate for the unstable characteristics in L_{vcm}. To do so, the gain of L_{vcm} should be canceled by the L_{mil} (open-loop for Milli actuator) from 2 to 4 kHz. It must also provide the low-pass effect so that the gain of L_{mil} has low gain in high frequency range. As a result, C_{mil} is given as shown by solid lines in Fig. 10.

C_{mic} has to compensate for the characteristics of the control system from 4 to 8 kHz. It must also provide the low-pass effect so that the gain of L_{mic} (open-loop for the Micro actuator) has low gain in high-frequency range. As a result, C_{mic} is given as shown by dashed lines in Fig. 10.

Fig. 11 shows the frequency responses of the open-loop characteristics in the Case 1 (dot: L_{tsa}, solid: L_{vcm}, dashed: L_{mil}, dot-dashed: L_{mic}). Fig. 12 shows the gain frequency responses of the closed-loop characteristics in the Case 1 (solid: S_{tsa}, dashed: R_{mil}, dot-dashed: R_{mic}). This figure indicates that the designed control system meets the design constrains for the closed-loop characteristics. This figure also indicates that the upper limits for $||S_{tsa}||_\infty$ is the bottleneck for the servo bandwidth of the triple-stage actuator system. On the other hand, the upper limit for $||R_{mil}||_\infty$ or $||R_{mic}||_\infty$ are not the bottleneck.

3.2 Case 2: "VCM + Milli + Thermal"

Fig. 13 shows a block diagram of a magnetic-head positioning control system with the triple-stage-actuator that consists of the VCM, the Milli actuator, and the Thermal actuator. Here, C_{the} is a feedback controller for the Thermal actuator, u_{the} is an output signal from C_{the}, and y_{the} is an output signal from P_{the}.

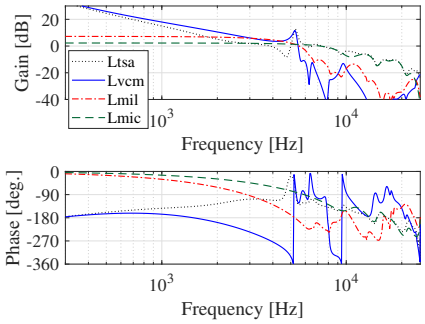

Fig. 11. Frequency responses of L_{tsa}, L_{vcm}, L_{mil}, and L_{mic} in Case 1.

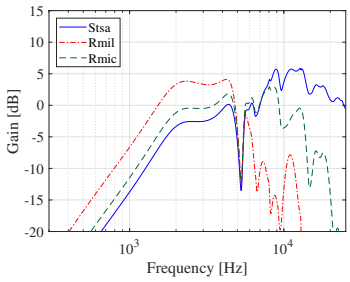

Fig. 12. Gain frequency responses of S_{tsa}, R_{mil}, and R_{mic} in Case 1.

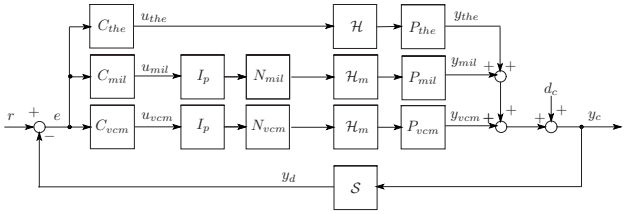

Fig. 13. Block diagram of control system in Case 2: "VCM + Milli + Thermal".

The open-loop characteristics for the Thermal actuator (L_{the}), can be given as follows.

$$L_{the}[\omega_0] = C_{the}[e^{j\omega_0 T_s}]P_{dthe}[\omega_0], \tag{8}$$

where

$$P_{dthe}[\omega] = \frac{1}{T_s}\sum_{k=-\infty}^{\infty} P_{the}(j\omega + j\omega_s k)\mathcal{H}(\omega + \omega_s k). \tag{9}$$

The open-loop characteristics in the triple-stage actuator system (L_{tsa}) and the stroke function for the Thermal actuator (R_{the}), can be given by following equations.

$$L_{tsa} = L_{vcm} + L_{mil} + L_{the},\ R_{the} = L_{the} \cdot S_{tsa}. \tag{10}$$

In order not to exceed the stroke limitations of the actuators, we have set the upper limit of $||R_{the}||_\infty$ as 0 dB.

Fig. 14 shows the frequency responses of the feedback controllers in the Case 2 (solid: C_{vcm}, dashed: C_{mil}, dot-dashed: C_{the}). Fig. 7 shows that the Thermal actuator has little adverse effect from mechanical resonances. However, the Thermal actuator's stoke is too short to compensate for the disturbances caused by the external vibrations at low frequency. Thus, C_{the} has to provide the high-pass effect except around the Nyquist frequency.

Fig. 15 shows the frequency responses of the open-loop characteristics in the Case 2 (dot: L_{tsa}, solid: L_{vcm},

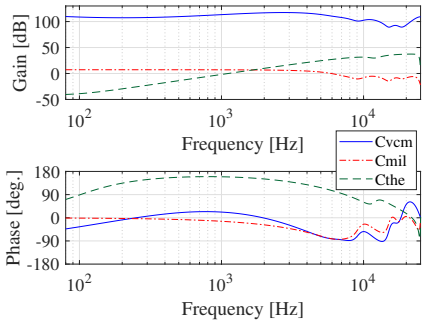

Fig. 14. Frequency responses of C_{vcm}, C_{mil}, and C_{the} in Case 2.

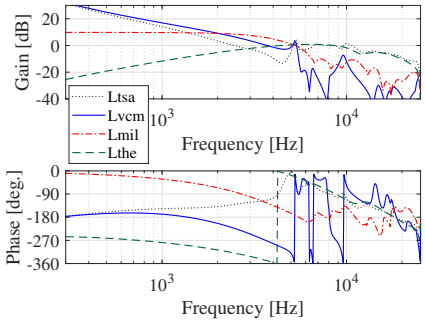

Fig. 15. Frequency responses of L_{tsa}, L_{vcm}, L_{mil}, and L_{the} in Case 2.

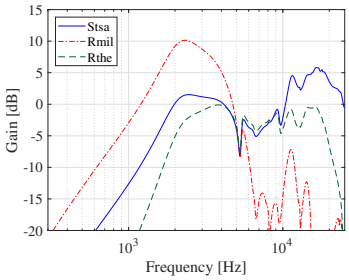

Fig. 16. Gain frequency responses of S_{tsa}, R_{mil}, and R_{the} in Case 2.

dashed: L_{mil}, dot-dashed: L_{the}). This figure indicates that the open-loop of the Thermal actuator plays the main role in the triple-stage actuator system above 8 kHz. Fig. 16 shows the gain frequency responses of the closed-loop characteristics in the Case 2 (solid: S_{tsa}, dashed: R_{mil}, dot-dashed: R_{the}). Fig. 16 indicates that the upper limits for $||S_{tsa}||_\infty$ and $||R_{the}||_\infty$ are the bottleneck for the servo bandwidth of the triple-stage actuator system.

3.3 Case 3: "VCM + Micro + Thermal"

Fig. 17 shows a block diagram of a magnetic-head positioning control system with the triple-stage-actuator that consists of the VCM, the Micro actuator, and the Thermal actuator.

An open-loop characteristics L_{tsa} is given as follows.

$$L_{tsa} = L_{vcm} + L_{mic} + L_{the}. \tag{11}$$

Fig. 18 shows the frequency responses of the feedback controllers in the Case 3 (solid: C_{vcm}, dashed: C_{mic}, dot-dashed: C_{the}). Fig. 19 shows the frequency responses of the

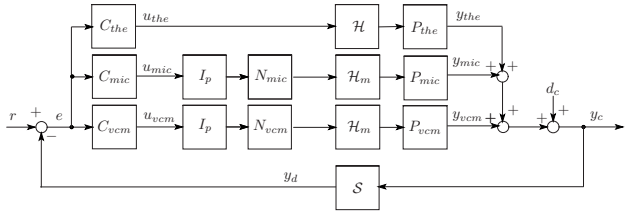

Fig. 17. Block diagram of control system in Case 3: "VCM + Micro + Thermal".

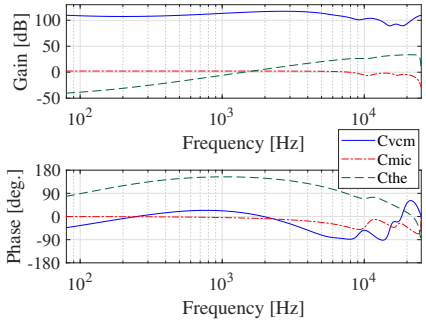

Fig. 18. Frequency responses of C_{vcm}, C_{mic}, and C_{the} in Case 3.

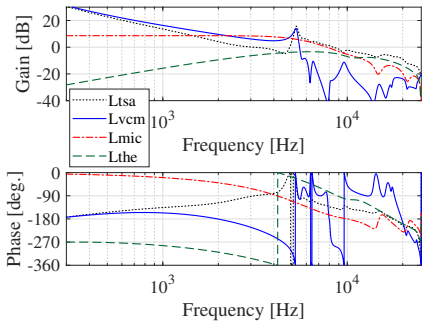

Fig. 19. Frequency responses of L_{tsa}, L_{vcm}, L_{mic}, and L_{the} in Case 3.

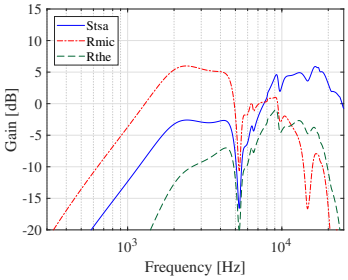

Fig. 20. Gain frequency responses of S_{tsa}, R_{mic}, and R_{the} in Case 3.

open-loop characteristics in the Case 3 (dot: L_{tsa}, solid: L_{vcm}, dashed: L_{mic}, dot-dashed: L_{the}). Fig. 20 shows the gain frequency responses of the closed-loop characteristics in the Case 3 (solid: S_{tsa}, dashed: R_{mic}, dot-dashed: R_{the}). Fig. 20 indicates that the upper limits for $||S_{tsa}||_\infty$ and $||R_{mic}||_\infty$ are the bottleneck for the servo bandwidth of the triple-stage actuator system.

4. PERFORMANCE COMPARISON

To verify the performances of the designed three control systems, we performed time-domain simulations of the

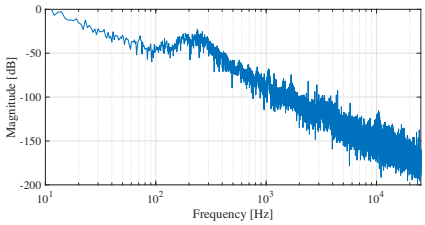

Fig. 21. Amplitude spectrum of external vibration.

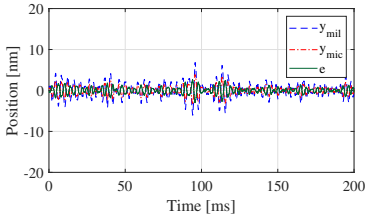

(a) Case 1

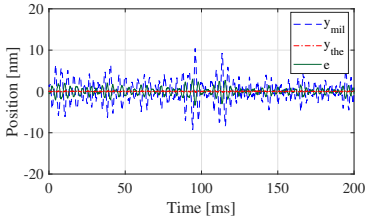

(b) Case 2

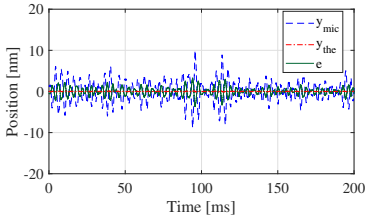

(c) Case 3

Fig. 22. Simulation results of e, y_{mil}, y_{mic}, and y_{the}.

track-following control under the external vibration. Here, the reference signal r is set as 0, and the disturbance signal d_c is set as a measured external vibration by using acceleration sensors in an actual file server. Fig. 21 shows an amplitude spectrum of the d_c. By employing the measured controlled objects and the disturbance source, this simulation result seems to be similar to an experimental result (Atsumi et al. (2013)).

Fig. 22 (a) shows the simulation results of the Case 1 (solid: y_c, dashed: y_{mil}, dot-dashed: y_{mic}). Fig. 22 (b) shows the simulation results of the Case 2 (solid: y_c, dashed: y_{mil}, dot-dashed: y_{the}). Fig. 22 (c) shows the simulation results of the Case 3 (solid: y_c, dashed: y_{mic}, dot-dashed: y_{the}). The 3σ values of y_c, y_{mil}, y_{mic}, and y_{the} are listed in Table 1. In this comparison between three triple-stage actuator systems, the case with "VCM + Milli + Micro" has the best performance because other two systems have large negative impacts from the upper limits for stroke functions of the Micro or Thermal actuators below 3 kHz as shown in Figs. 16 and 20 .

5. CONCLUSION

In order to find the best triple-stage actuator system for upcoming 1000 kTPI (track pitch: 25 nanometer) HDD era, we present a comparison study between three triple-stage actuator systems: "VCM + Milli + Micro", "VCM + Milli + Thermal", and "VCM + Micro + Thermal". Results of performance evaluations of the track-following control systems under the external vibration show that achievable disturbance-rejection performances of these triple-stage-actuator systems depend on not only the frequency responses the actuators but also the stroke limitations of the actuators. As a result, we found that the triple-stage actuator system that consist of the VCM, the Milli actuator, and the Micro actuator has the best performance for 1000 kTPI HDD.

Table 1. 3 σ values of y_c, y_{mil}, y_{mic}, and y_{the}.

	y_c	y_{mil}	y_{mic}	y_{the}
Case 1	2.270 nm	5.215 nm	2.952 nm	–
Case 2	2.551 nm	7.892 nm	–	0.180 nm
Case 3	2.808 nm	–	7.594 nm	0.120 nm

ACKNOWLEDGEMENT

A part of this work is supported by JSPS KAKENHI Grant Number JP18K04210.

REFERENCES

Abrahamson, S. and Fu-ying, H. (2015). Towards a million TPI. In *Proceedings of JSME-IIP/ASME-ISPS Joint Conference on Micromechatronics for Information and Precision Equipment : IIP/ISPS joint MIPE*, TuW–1.

Atsumi, T. (2010). Disturbance Suppression beyond Nyquist Frequency in Hard Disk Drives. *Mechatronics*, 20(1), 67–73.

Atsumi, T. (2016). Emerging Technology for Head-Positioning System in HDDs. *IEEJ Journal of Industry Applications*, 5(2), 117–122.

Atsumi, T. and Messner, W.C. (2013). Estimation Method for Unobservable Settling Vibration of Head-Positioning Control in Hard Disk Drives. *Mechatronics*, 23(1), 37–45.

Atsumi, T., Nakamura, S., Odai, M., Naniwa, I., and Nosaki, S. (2013). Experimental Evaluation of Triple-Stage-Actuator System with Thermal Actuator for Hard Disk Drives. *Journal of Advanced Mechanical Design, Systems, and Manufacturing*, 7(4), 722–735.

Atsumi, T., Suzuki, K., Nakamura, S., and Ohta, M. (2015). Vibration Control with Thin-Film-Coil Actuator for Head-Positioning System in Hard Disk Drives. *Journal of Advanced Mechanical Design, Systems, and Manufacturing*, 9(1), JAMDSM0010.

Herrmann, G., C. Turner, M., Postlethwaite, I., and Guo, G. (2004). Practical Implementation of a Novel Anti-Windup Scheme in a HDD-Dual-Stage Servo-System. *Mechatronics, IEEE/ASME Transactions on*, 9, 580 – 592.

HGST (2017). TECH BRIEF: HGST Micro Actuator. TB02–HGST–Micro–Actuator–EN–US–0917–02. URL `https://www.westerndigital.com/`.

Yamaguchi, T. and Atsumi, T. (2008). HDD Servo Control Technologies - What we have done and where we should go - (Keynote). In *Proceedings of The 17th World Congress The International Federation of Automatic Control*, 821–826.